Kinematic Resolutions for ν_μ-CC and ν_μ-CC QEL Events in the Near Detector

Mark Dorman

July 22nd, 2008

Abstract

Samples of ν_μ-CC and ν_μ-CC QEL events are selected in the ND and MC truth information is used to calculate resolutions and biases in the reconstruction of a number of variables.

1 Sample Definitions

The analysis uses `cedar_phy_bhcurv daikon04` MC with the appropriate energy corrections applied and no beam, hadron production, detector parameter or generator weighting has been used. The total exposure of the MC sample is 5.84e19 POT and the following pre-selection criteria have been applied:

- **Fiducial volume:** the event vertex must be located within a 1m radius about the beam spot and between 1 and 5m along the z-direction.
- **Number of tracks:** the event must contain one or more tracks.
- **Track quality**: the reconstructed track must either pass the internal checks of the track fitter or satisfy all of the following conditions (track reclamation scheme):
  - The difference in the track vertex plane between the U and V views is less than 6 planes.
  - The difference in the track end plane between the U and V views is less than 41 planes.
  - The number of the track end plane must be less than 270.

A further two cuts are applied to define a ν_μ-CC-like sample:

- **Track charge-sign**: the reconstructed track must have negative charge-sign.
- **CC-like**: the reconstructed events must take a KNN PID value of greater than 0.3.

In addition to these selection cuts, MC truth information is then used to select the samples of true ν_μ-CC and true ν_μ-CC QEL events that are used in the resolution fitting analysis.

2 Resolution Fitting Method

The resolution analysis proceeds by considering distributions of reconstructed minus truth $(R-T)$ or reconstructed minus truth all divided by truth $((R-T)/T)$ variables in a number of slices of a certain truth variable. In each of these slices the $R-T$ or $(R-T)/T$ distribution is fitted with a log-normal distribution which may be written as:

$$f(x,\mu,\sigma,t,N) = Nexp\left\{-\frac{1}{2}\left[\log\left(1+t\left(\frac{x-\mu}{\sigma}\right)\frac{\sinh(tK)}{tK}\right)\right]^2+\frac{t^2}{2}\right\} \quad (1)$$

where $K=\sqrt{\log(4)}$, x is the variable in question, μ is the mean, σ is the width, t is a tail parameter and N a normalisation factor. This functional form describes a Gaussian distribution with a one-sided tail. In the limit that $t \simeq 0$ the fitted function is given by:

$$f(x,\mu,\sigma) \propto Nexp\left[-\frac{1}{2}\left(\frac{x-\mu}{\sigma}\right)^2\right] \quad (2)$$

Figure 1 shows an example of the fitted $R-T$ Q^2 distributions for true ν_μ-CC events in the CC-like sample in a number of slices of true Q^2.

In most cases the log-normal form provides a better estimate of the mean and width than can be obtained either directly from the distributions (or via a standard Gaussian fit) by neglecting the contributions of the tails of the $R-T$ or $(R-T)/T$ distributions. The Gaussian means from the log-normal fits correspond to the pull on the resolution and provide an estimate for the accuracy of the reconstruction. The Gaussian widths provide an estimate of the resolution (precision of the reconstruction) for the variable in question. The fit results for the $R-T$ distributions provide estimate of the absolute resolution and bias in each variable whereas the fit results for the $(R-T)/T$ distributions provide estimates of the fractional resolutions and biases. The Gaussian widths fitted in each slice can then be plotted as a function of the truth variable in question and this distribution fitted to provide a functional form to describe the detector resolution.

3 Results

3.1 Event Vertex Position Resolution

Figures 2 and 3 show the fitted resolutions and biases in the reconstruction of event vertex positions as a function of the x and y coordinates. Similar plots as a function of the z coordinate are not shown due to the inherent quantisation introduced by the spectrometer portion of the detector. It can be seen that the vertex resolution for true ν_μ-CC QEL events is slightly better than that for the whole true ν_μ-CC event sample and this difference is attributed to the cleaner hadronic environment associated with QEL interactions. It is also worth noting that the vertex position resolution is flat as a function of both the x and y coordinates and the bias is everywhere much smaller than the resolution.

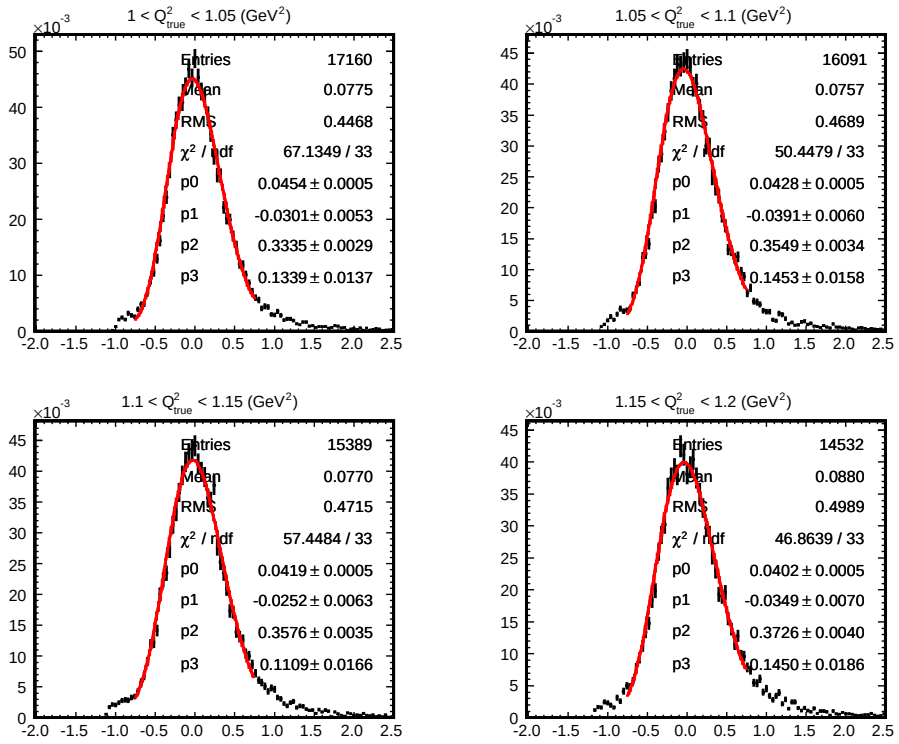

Figure 1: *Distributions of $R-T$ Q^2 for true ν_μ-CC events in the CC-like sample in four slices of true Q^2. The red lines show the fitted log-normal distributions and the parameter p0 corresponds to the overall normalisation, p1 to the Gaussian mean, p2 to the Gaussian width and p3 to the tail parameter.*

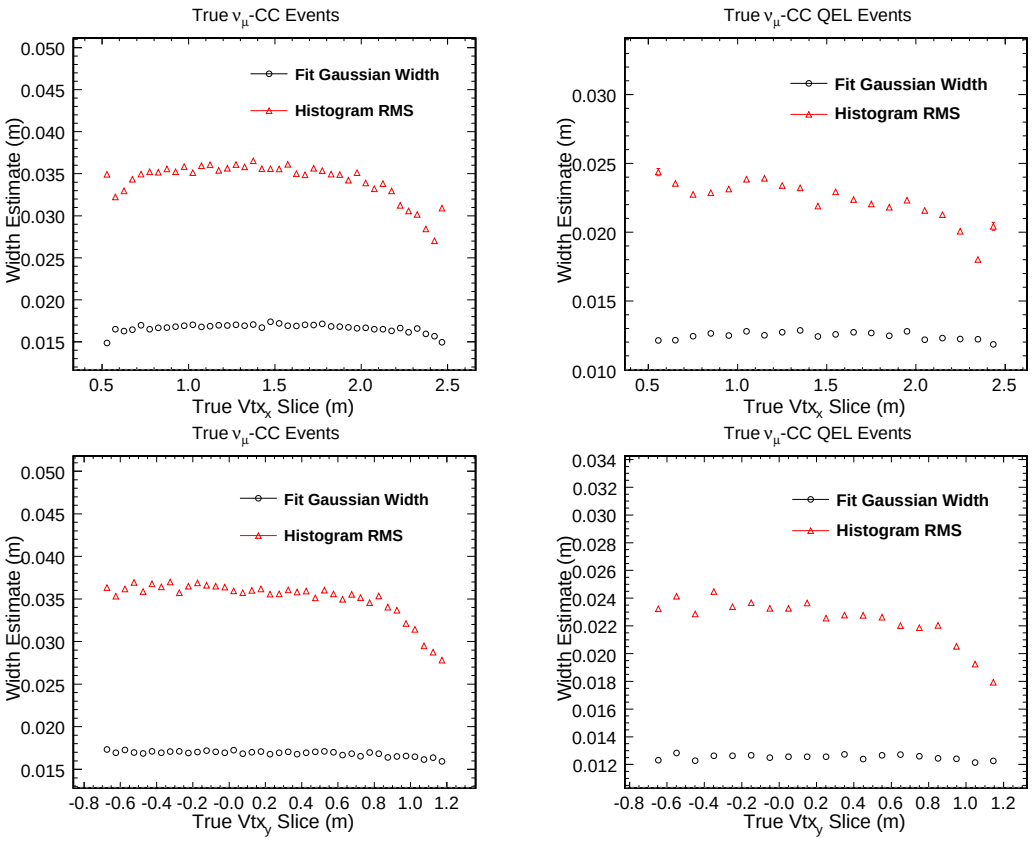

Figure 2: *The left-hand figures correspond to true ν_μ-CC events in the CC-like sample whilst the right-hand figures correspond to true ν_μ-CC QEL events in the CC-like sample. The figures show the Gaussian widths from the log-normal fits to the $R-T$ distributions as black circles along with the RMS values of the $R-T$ histograms as red triangles. The top plots correspond to the vertex x coordinate whilst the bottom plots correspond to the vertex y coordinate. All points are plotted at the mean value of the true vertex position in a given slice rather than at the centre of that slice and the differences between the black circles and red triangles correspond to the influence of the tails of the $R-T$ or $(R-T)/T$ distributions.*

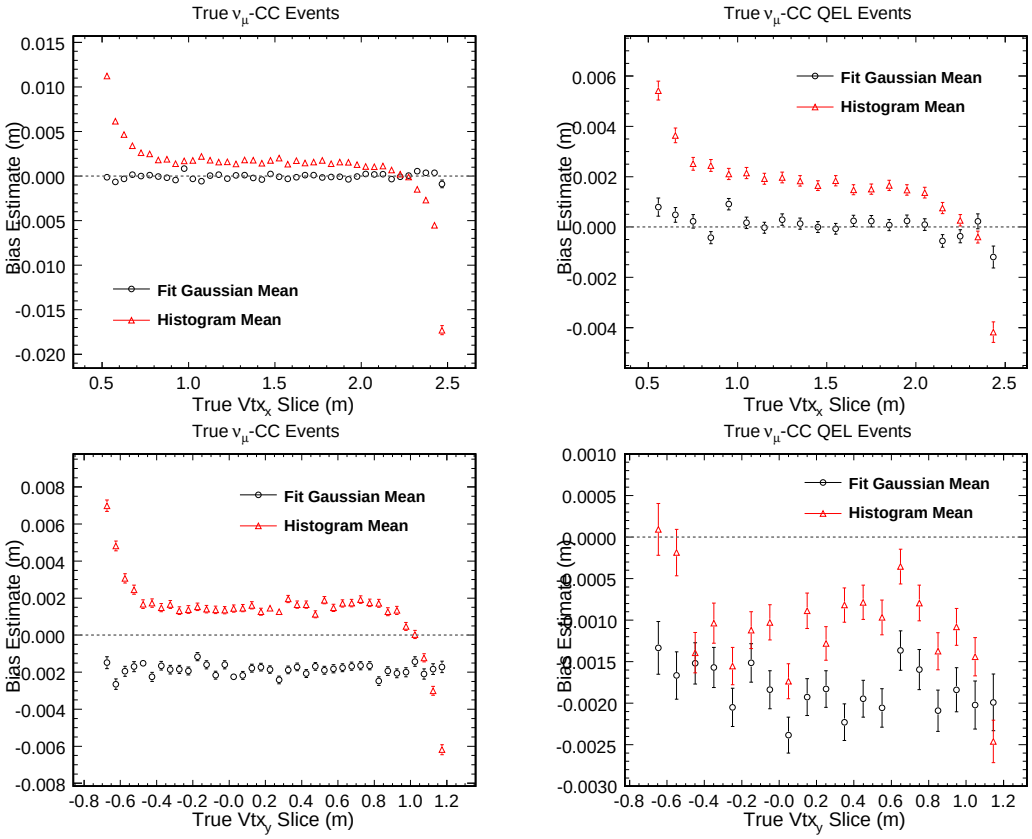

Figure 3: *The left-hand figures correspond to true ν_μ-CC events in the CC-like sample whilst the right-hand figures correspond to true ν_μ-CC QEL events in the CC-like sample. The figures show the Gaussian means from the log-normal fits to the $R-T$ distributions as black circles along with the mean values of the $R-T$ histograms as red triangles. The top plots correspond to the vertex x coordinate whilst the bottom plots correspond to the vertex y coordinate. All points are plotted at the mean value of the true vertex position in a given slice rather than at the centre of that slice and the differences between the black circles and red triangles correspond to the influence of the tails of the $R-T$ or $(R-T)/T$ distributions.*

3.2 E_μ Resolution for Stopping Muons as Measured by Range

The muon energy resolution is broken down into two classes; the resolution for muons that stop in the detector and whose momentum is measured using range and the resolution for muons that exit the detector and whose momentum is measured by curvature in the magnetic field. Figure 5 shows the fitted Gaussian means and widths for stopping muons as a function of true muon energy for true ν_μ-CC events in the CC-like sample and for ν_μ-CC QEL events in the CC-like sample.

It can be seen that generally there is good agreement between the resolutions and biases for true ν_μ-CC and true ν_μ-CC QEL events although the resolution is slightly better for the true ν_μ-CC QEL events at low muon energies. This is again attributed to the cleaner hadronic environment of the QEL interactions with mis-placement of the vertex being more likely for RES and DIS interactions. At higher muon energies the resolution becomes slightly worse because a greater fraction of tracks are ending in the spectrometer where accurate determination of the track end plane is more difficult.

3.3 E_μ Resolution for Exiting Muons as Measured by Curvature

Figure 6 shows the fitted Gaussian means and widths for exiting muons as a function of true muon energy for true ν_μ-CC events in the CC-like sample and for ν_μ-CC QEL events in the CC-like sample. It can be seen that the log-normal fits for the true ν_μ-CC QEL events in the true muon energy region around 5 GeV do not result in a good fit and figure 4 shows that the lack of statistics is the cause of this problem.

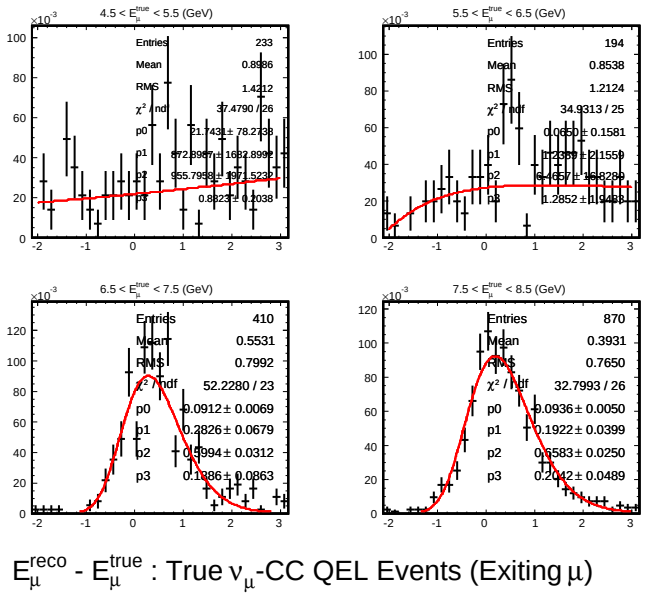

Figure 4: *Distributions of $R-T$ E_μ for true ν_μ-CC QEL exiting muon events in the CC-like sample in four slices of true E_μ. The red lines show the fitted log-normal distributions and the parameter $p0$ corresponds to the overall normalisation, $p1$ to the Gaussian mean, $p2$ to the Gaussian width and $p3$ to the tail parameter.*

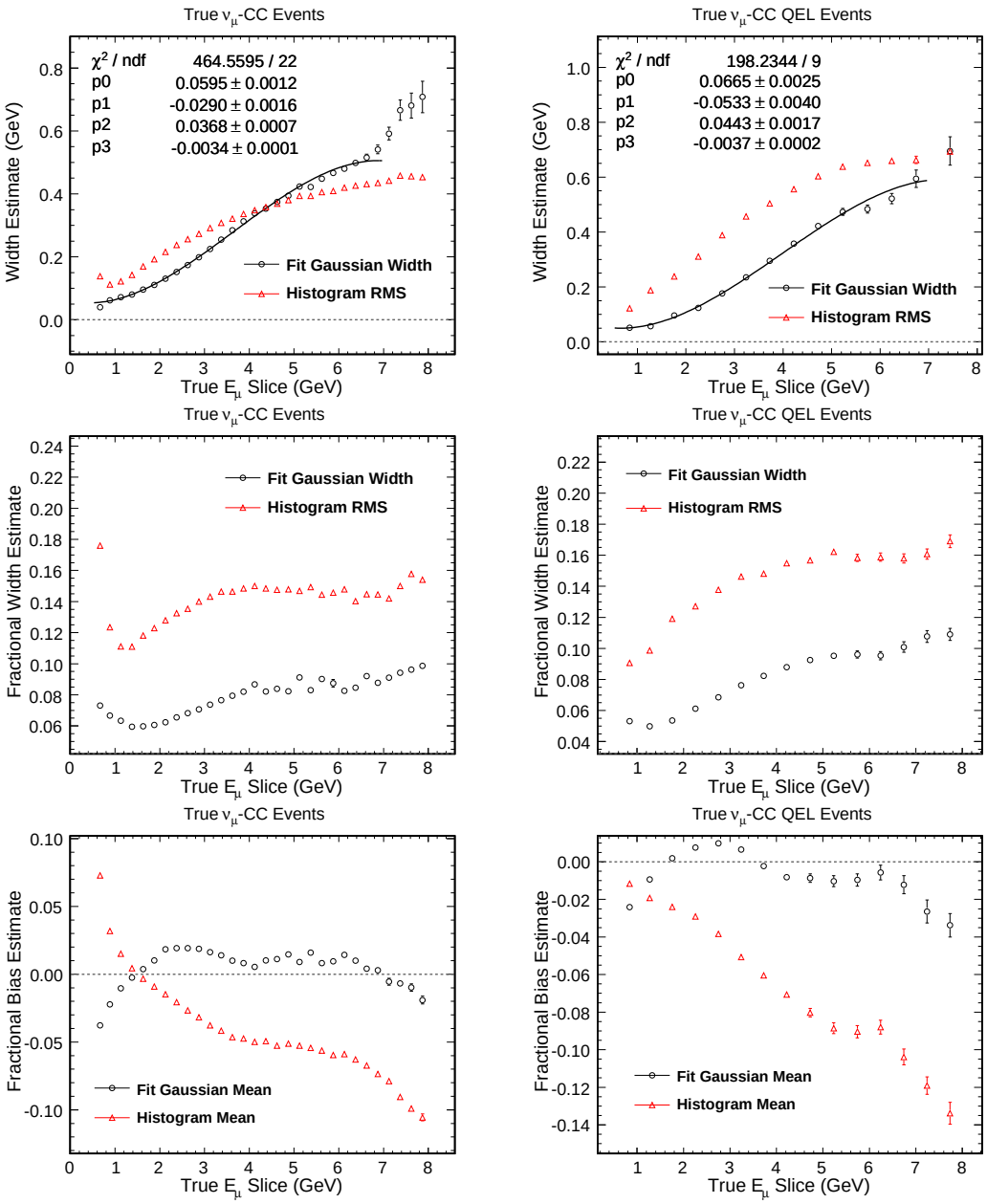

Figure 5: **Stopping muon energy resolution.** *The left-hand figures correspond to true ν_μ-CC events in the CC-like sample whilst the right-hand figures correspond to true ν_μ-CC QEL events in the CC-like sample. The top figures show the Gaussian widths from the log-normal fits to the $R-T$ distributions as black circles along with the RMS values of the $R-T$ histograms as red triangles. The black curves correspond to a fitted third order polynomial parameterisation of the detector resolution and all points are plotted at the mean value of the true muon energy in a given slice rather than at the centre of that slice to make the parameterisations more accurate. The second row of figures show the fractional fitted Gaussian widths and $(R-T)/T$ histogram RMS values whilst the bottom row of figures show the fractional fitted Gaussian means and $(R-T)/T$ histogram means. The differences between the black circles and red triangles correspond to the influence of the tails of the $R-T$ or $(R-T)/T$ distributions.*

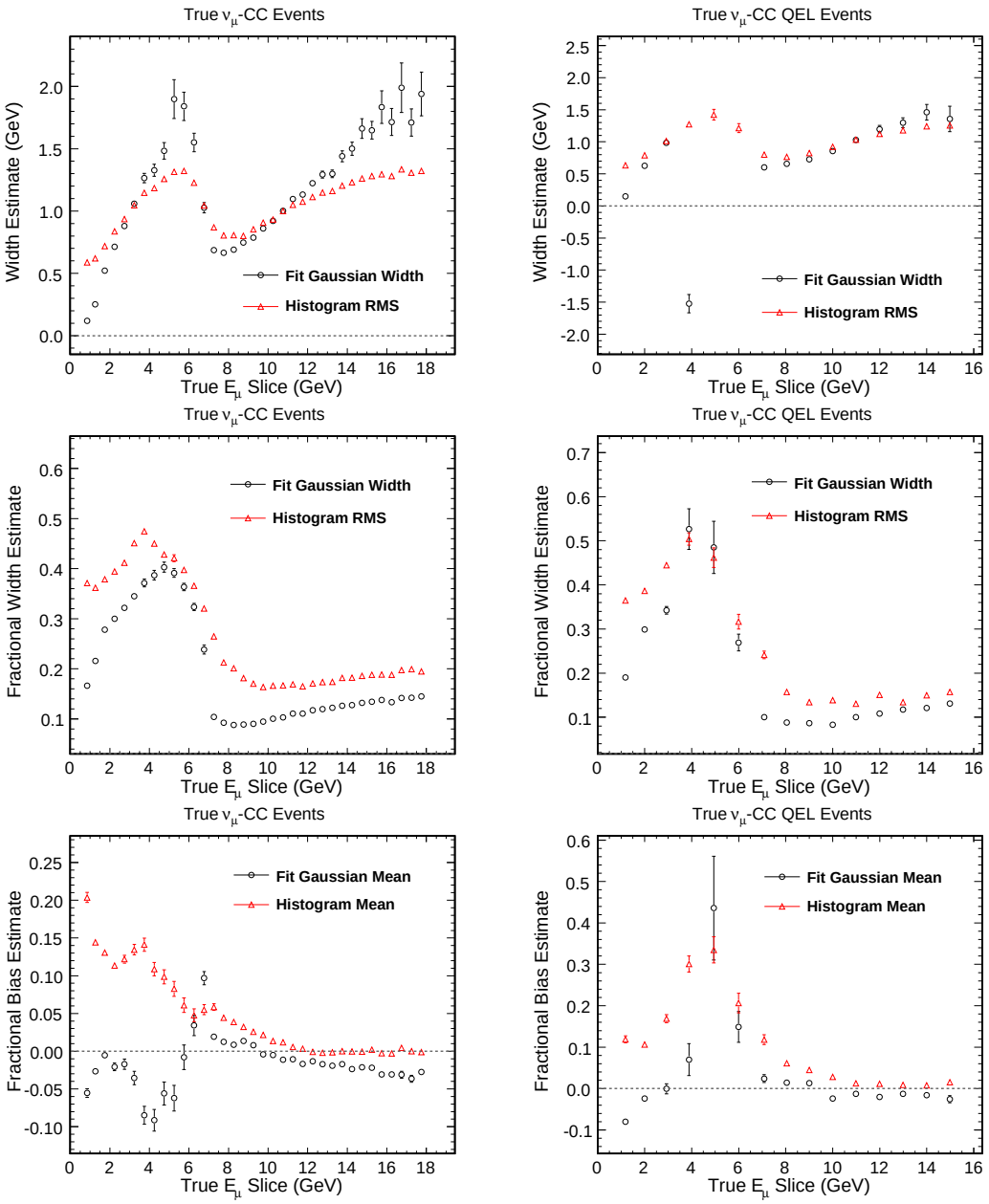

Figure 6: **Exiting muon energy resolution.** *The left-hand figures correspond to true ν_μ-CC events in the CC-like sample whilst the right-hand figures correspond to true ν_μ-CC QEL events in the CC-like sample. The top figures show the Gaussian widths from the log-normal fits to the $R-T$ distributions as black circles along with the RMS values of the $R-T$ histograms as red triangles. All points are plotted at the mean value of the true muon energy in a given slice rather than at the centre of that slice. The second row of figures show the fractional fitted Gaussian widths and $(R-T)/T$ histogram RMS values whilst the bottom row of figures show the fractional fitted Gaussian means and $(R-T)/T$ histogram means. The differences between the black circles and red triangles correspond to the influence of the tails of the $R-T$ or $(R-T)/T$ distributions.*

The resolution for the energy of exiting muons has an interesting structure which corresponds to low energy muons that exit through the sides of the detector and higher energy muons that exit through the end of the detector. Fractionally the resolution is worst for the side-exiting lower energy muons for which there is a greater chance of a curvature mis-measurement due to the short track length. For end-exiting muons the fractional resolution becomes worse as the true muon energy increases because the tracks become straighter making an accurate curvature measurement more difficult.

3.4 E_{shw} Resolution

Figure 8 shows the fitted Gaussian means and widths as a function of the true shower energy for true ν_μ-CC events in the CC-like sample and for ν_μ-CC QEL events in the CC-like sample. Note that up to true shower energies of 300 MeV the $R-T$ and $(R-T)/T$ distributions are dominated by events where no hadronic energy was reconstructed inside the detector, as demonstrated in figure 7, and as such the log-normal form cannot adequately describe these distributions.

The fractional shower energy resolution improves with true shower energy as might be expected given that the mis-reconstruction of small numbers of strip hits has a smaller relative impact on the total reconstructed shower energy. It can also be seen that the resolution and bias are worse for the true ν_μ-CC QEL events, as opposed to the full ν_μ-CC sample, and this could be because often a large fraction of the shower energy in QEL interactions is contained in a single proton strip hit near to the event vertex which can more easily be mis-reconstructed as belonging to the main muon track.

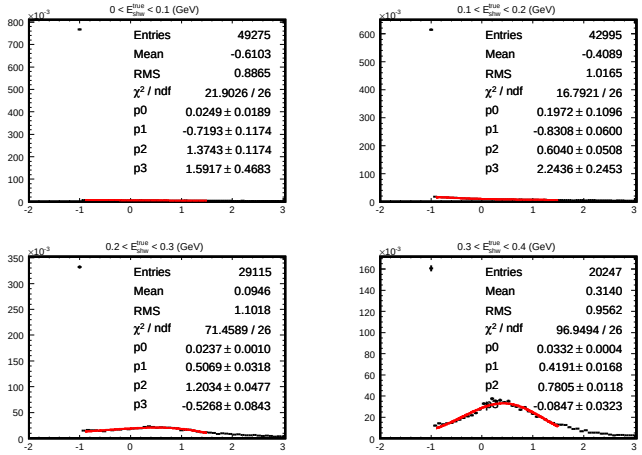

Figure 7: *Distributions of $(R-T)/T$ E_{shw} for true ν_μ-CC QEL events in the CC-like sample in four slices of true E_{shw}. The red lines show the fitted log-normal distributions and the parameter $p0$ corresponds to the overall normalisation, $p1$ to the Gaussian mean, $p2$ to the Gaussian width and $p3$ to the tail parameter.*

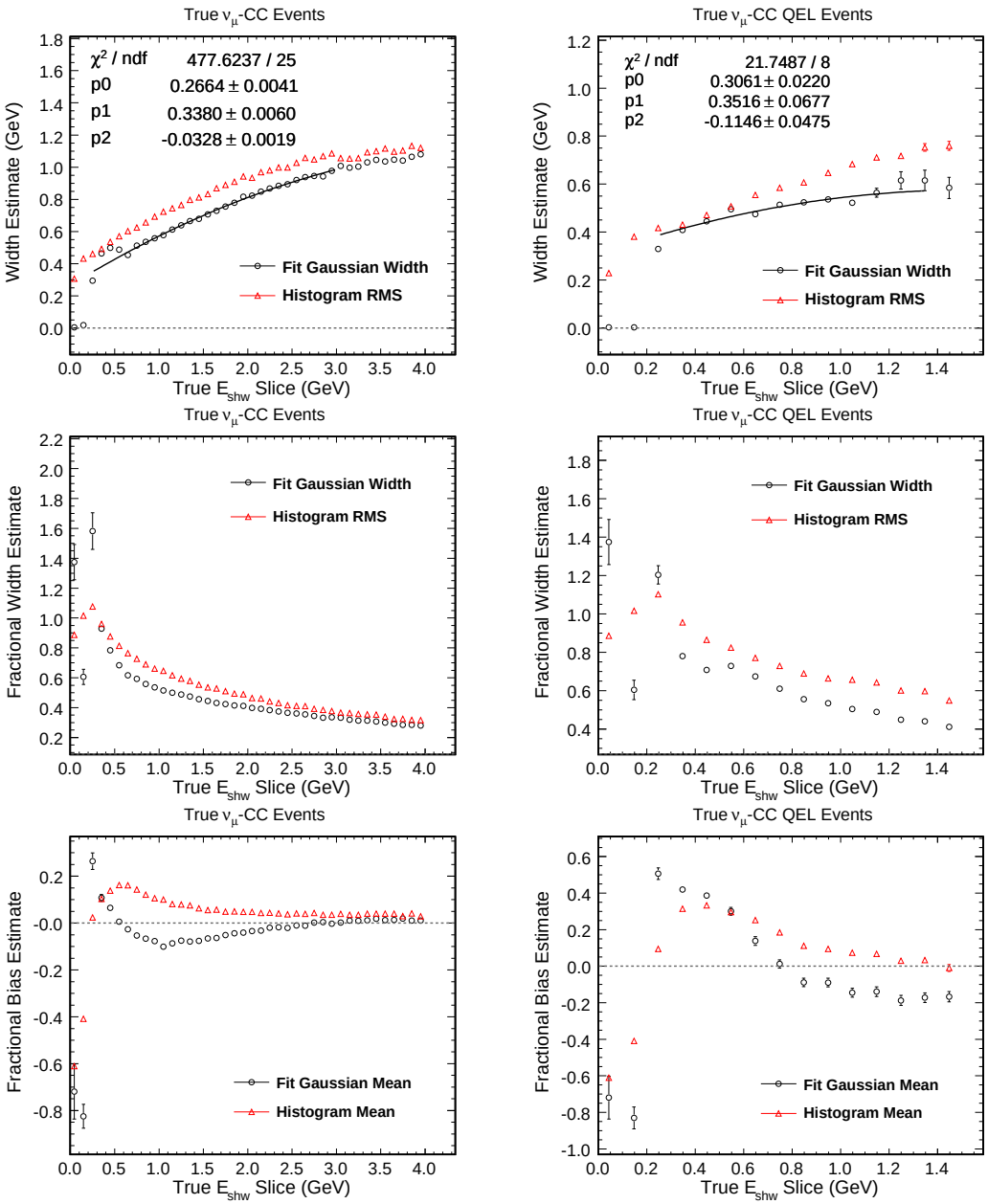

Figure 8: **Shower energy resolution.** *The left-hand figures correspond to true ν_μ-CC events in the CC-like sample whilst the right-hand figures correspond to true ν_μ-CC QEL events in the CC-like sample. The top figures show the Gaussian widths from the log-normal fits to the $R-T$ distributions as black circles along with the RMS values of the $R-T$ histograms as red triangles. The black curves correspond to a fitted second order polynomial parameterisation of the detector resolution and all points are plotted at the mean value of the true muon energy in a given slice rather than at the centre of that slice to make the parameterisation more accurate. The second row of figures show the fractional fitted Gaussian widths and $(R-T)/T$ histogram RMS values whilst the bottom row of figures show the fractional fitted Gaussian means and $(R-T)/T$ histogram means. The differences between the black circles and red triangles correspond to the influence of the tails of the $R-T$ or $(R-T)/T$ distributions.*

3.5 Muon Angle Resolution

The resolution and bias for the reconstruction of the muon opening angle with respect to the neutrino direction is shown both as a function of the true muon energy (in figure 9) and as a function of the true opening angle (in figure 10). The figures show that the bias for true ν_μ-CC QEL events is generally smaller than that of the true ν_μ-CC events (which is again attributed to the cleaner hadronic environment) whilst the resolutions are fairly comparable for the two samples. It should also be noted that, as with all of the variables considered so far, the fractional bias in the angle reconstruction is everywhere smaller than the fractional resolution.

3.6 E_ν Resolution

The next series of resolution and bias plots correspond to combined quantites that are defined in terms of the measured quantities whose resolutions and biases are presented above. Figure 11 shows the resolution and bias for the reconstructed neutrino energy (via the addition of the muon and shower energies) for true ν_μ-CC and true ν_μ-CC QEL events.

3.7 Q^2 Resolution

Figure 12 shows the resolution and bias for the reconstruction of Q^2 for true ν_μ-CC and true ν_μ-CC QEL events where:

$$Q^2 = 2E_\nu E_\mu(1-\cos(\theta_\mu)) \tag{3}$$

3.8 QEL-Assumed Kinematic Quantities

The final resolutions and biases to be presented in this document correspond to the QEL-assumed reconstruction of neutrino energy and squared four-momentum transfer and as such are only shown for the true ν_μ-CC QEL sample (see figure 13). These quantities are constructed using muon kinematics (and assuming that the hadronic system consists of a single proton) and, as can be shown via the conservation of four-momentum, are given by:

$$E_\nu^{QEL} = \frac{M_{nuc}E_\mu - \frac{M_\mu^2}{2}}{M_{nuc} - E_\mu + p_\mu\cos\theta_\mu} \tag{4}$$

where terms involving the binding energy of the struck nucleon in the nucleus have been neglected, and:

$$Q^2_{QEL} = -2E_\nu^{QEL}(E_\mu - p_\mu\cos\theta_\mu) + M_\mu^2 \tag{5}$$

It can be seen from figure 13 that the resolution (and to a lesser extent the bias) in the reconstruction of the neutrino energy is improved by the use of the QEL assumption whereas both methods of reconstructing the squared four-momentum transfer have similar resolutions and biases.

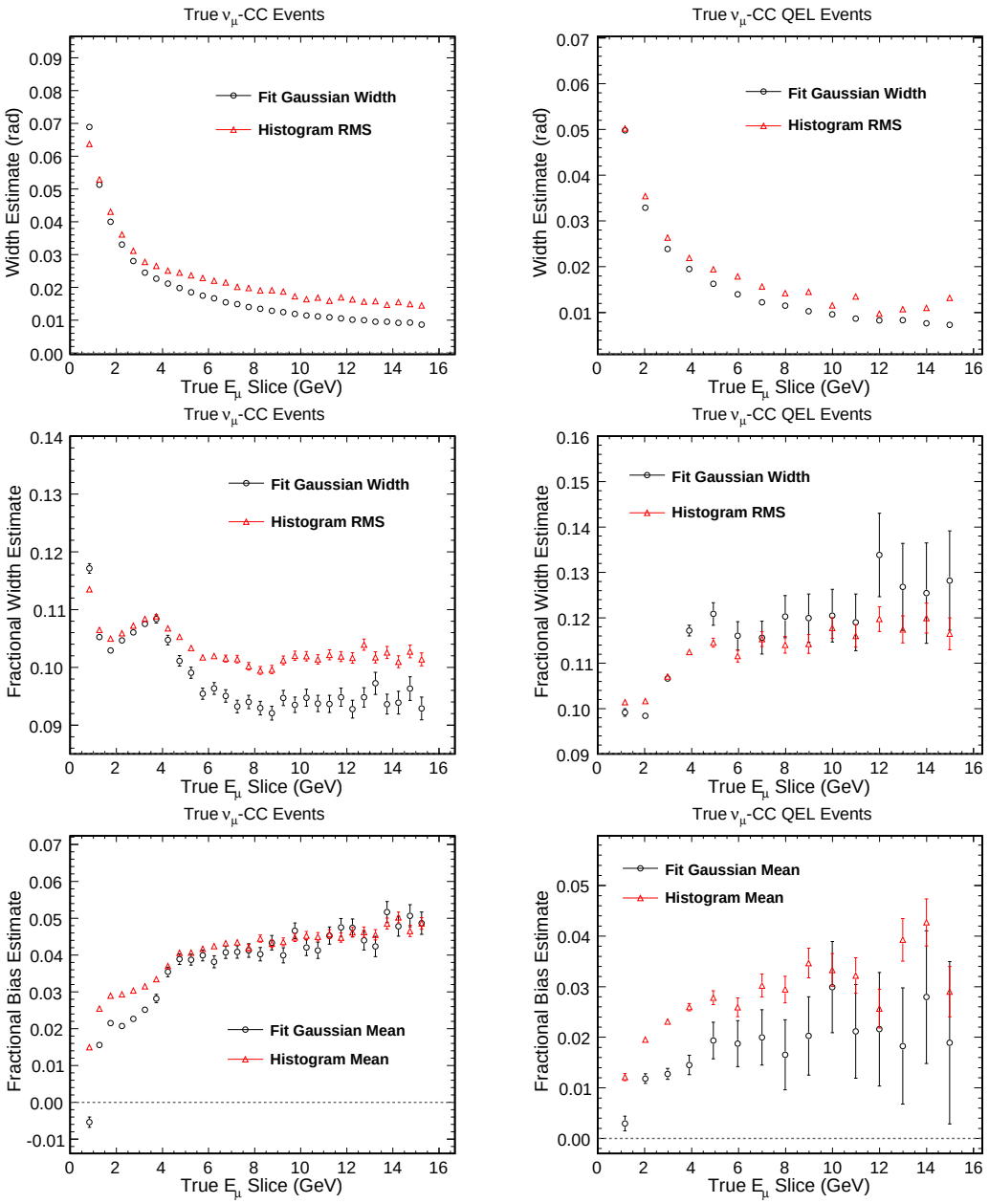

Figure 9: **Muon angle resolution as a function of true muon energy.** *The left-hand figures correspond to true ν_μ-CC events in the CC-like sample whilst the right-hand figures correspond to true ν_μ-CC QEL events in the CC-like sample. The top figures show the Gaussian widths from the log-normal fits to the $R-T$ distributions as black circles along with the RMS values of the $R-T$ histograms as red triangles. All points are plotted at the mean value of the true muon energy in a given slice rather than at the centre of that slice. The second row of figures show the fractional fitted Gaussian widths and $(R-T)/T$ histogram RMS values whilst the bottom row of figures show the fractional fitted Gaussian means and $(R-T)/T$ histogram means. The differences between the black circles and red triangles correspond to the influence of the tails of the $R-T$ or $(R-T)/T$ distributions.*

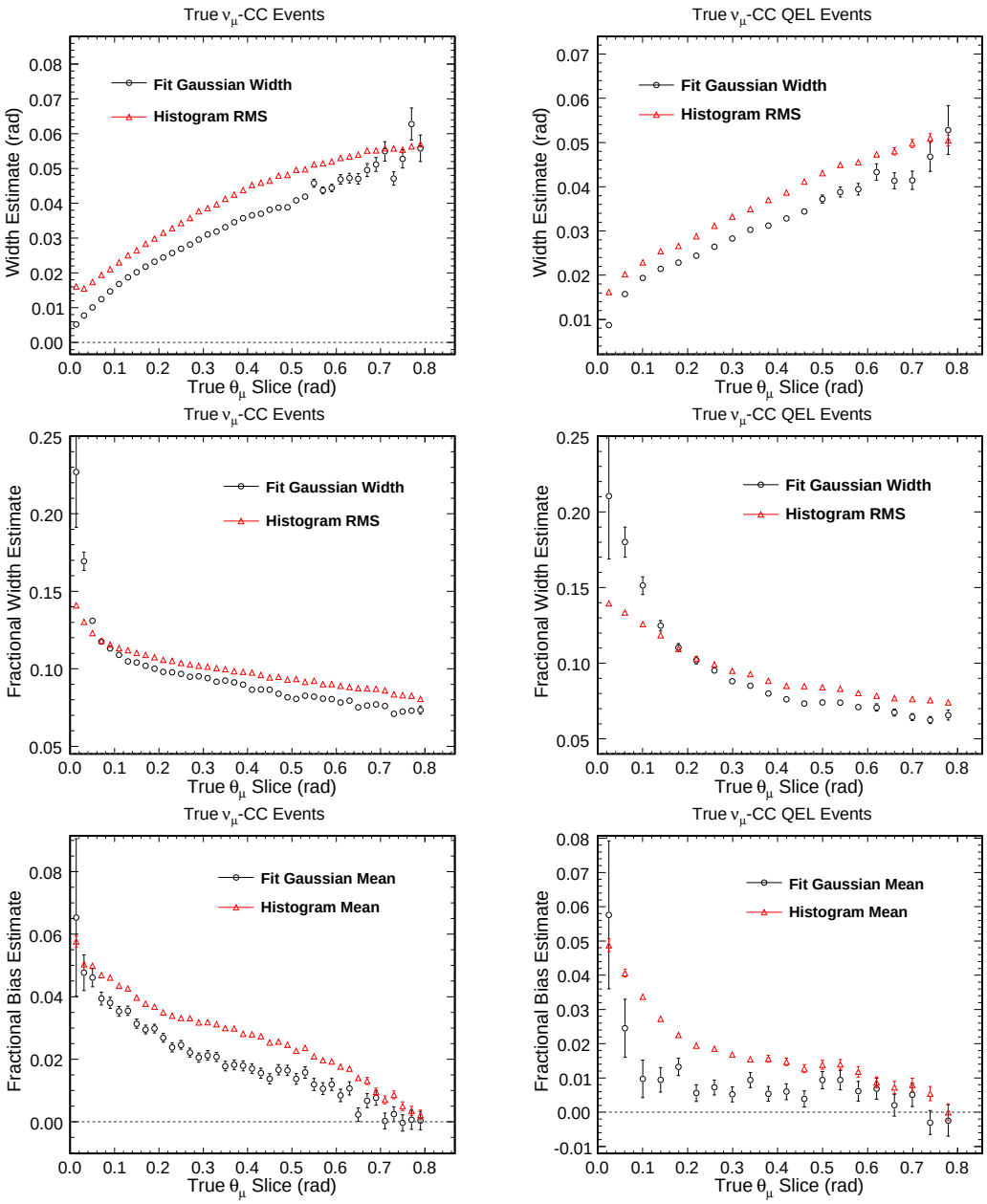

Figure 10: **Muon angle resolution as a function of true muon angle.** *The left-hand figures correspond to true ν_μ-CC events in the CC-like sample whilst the right-hand figures correspond to true ν_μ-CC QEL events in the CC-like sample. The top figures show the Gaussian widths from the log-normal fits to the $R-T$ distributions as black circles along with the RMS values of the $R-T$ histograms as red triangles. All points are plotted at the mean value of the true muon energy in a given slice rather than at the centre of that slice. The second row of figures show the fractional fitted Gaussian widths and $(R-T)/T$ histogram RMS values whilst the bottom row of figures show the fractional fitted Gaussian means and $(R-T)/T$ histogram means. The differences between the black circles and red triangles correspond to the influence of the tails of the $R-T$ or $(R-T)/T$ distributions.*

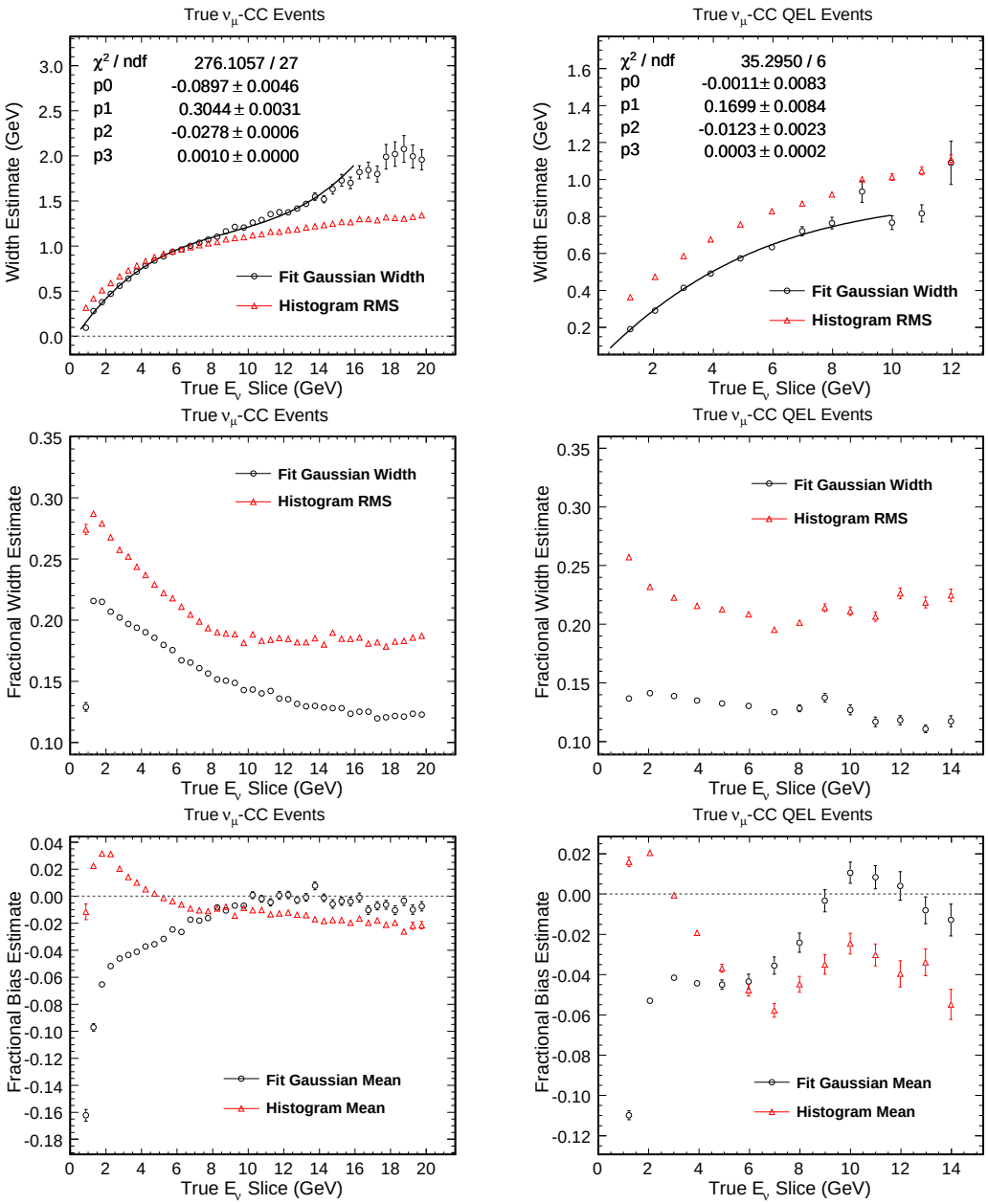

Figure 11: **Neutrino energy resolution.** *The left-hand figures correspond to true ν_μ-CC events in the CC-like sample whilst the right-hand figures correspond to true ν_μ-CC QEL events in the CC-like sample. The top figures show the Gaussian widths from the log-normal fits to the $R-T$ distributions as black circles along with the RMS values of the $R-T$ histograms as red triangles. The black curves correspond to a fitted third order polynomial parameterisation of the detector resolution and all points are plotted at the mean value of the true muon energy in a given slice rather than at the centre of that slice to make the parameterisation more accurate. The second row of figures show the fractional fitted Gaussian widths and $(R-T)/T$ histogram RMS values whilst the bottom row of figures show the fractional fitted Gaussian means and $(R-T)/T$ histogram means. The differences between the black circles and red triangles correspond to the influence of the tails of the $R-T$ or $(R-T)/T$ distributions.*

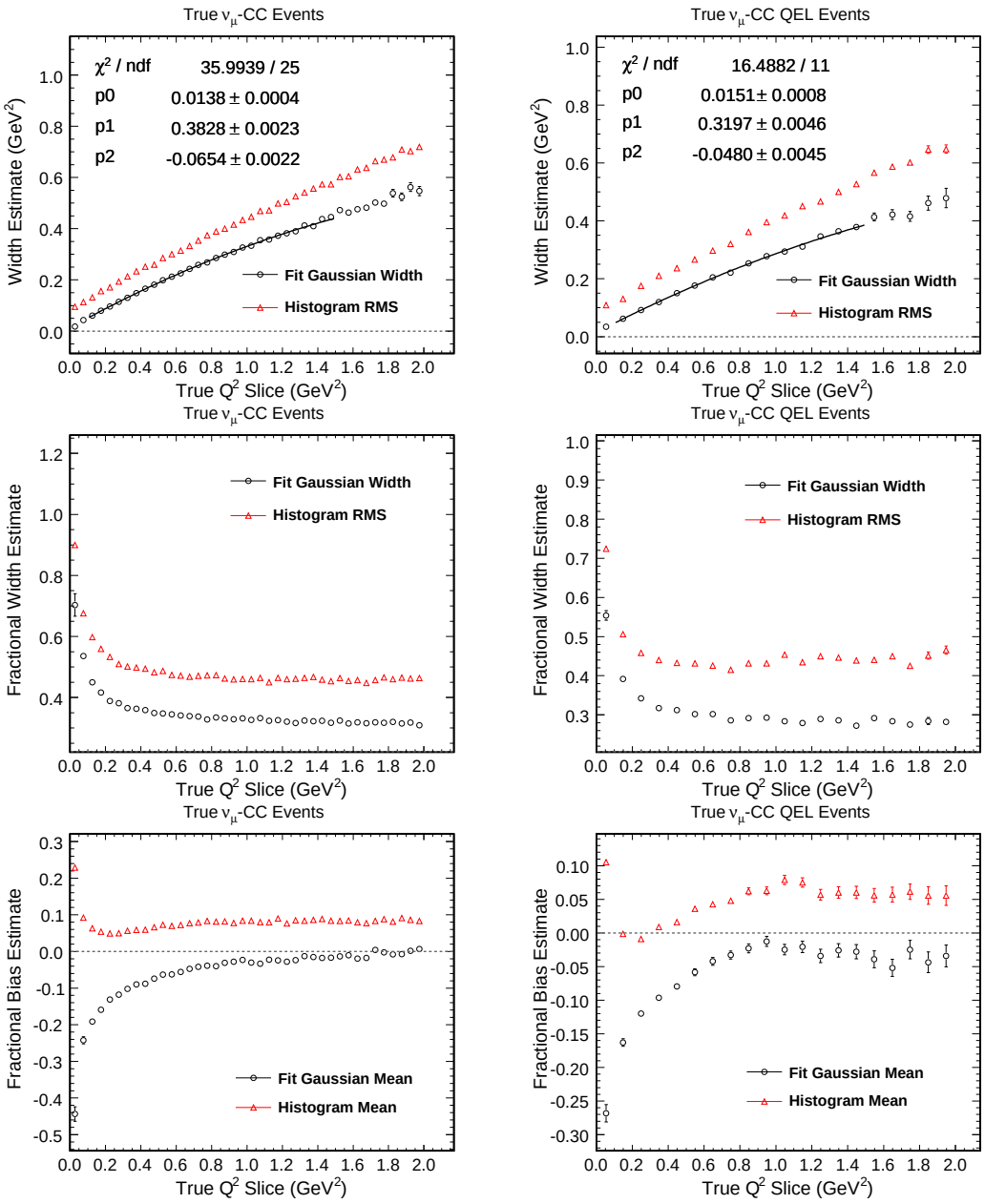

***Figure 12:* Q^2 resolution.** *The left-hand figures correspond to true ν_μ-CC events in the CC-like sample whilst the right-hand figures correspond to true ν_μ-CC QEL events in the CC-like sample. The top figures show the Gaussian widths from the log-normal fits to the $R-T$ distributions as black circles along with the RMS values of the $R-T$ histograms as red triangles. The black curves correspond to a fitted second order polynomial parameterisation of the detector resolution and all points are plotted at the mean value of the true muon energy in a given slice rather than at the centre of that slice to make the parameterisation more accurate. The second row of figures show the fractional fitted Gaussian widths and $(R-T)/T$ histogram RMS values whilst the bottom row of figures show the fractional fitted Gaussian means and $(R-T)/T$ histogram means. The differences between the black circles and red triangles correspond to the influence of the tails of the $R-T$ or $(R-T)/T$ distributions.*

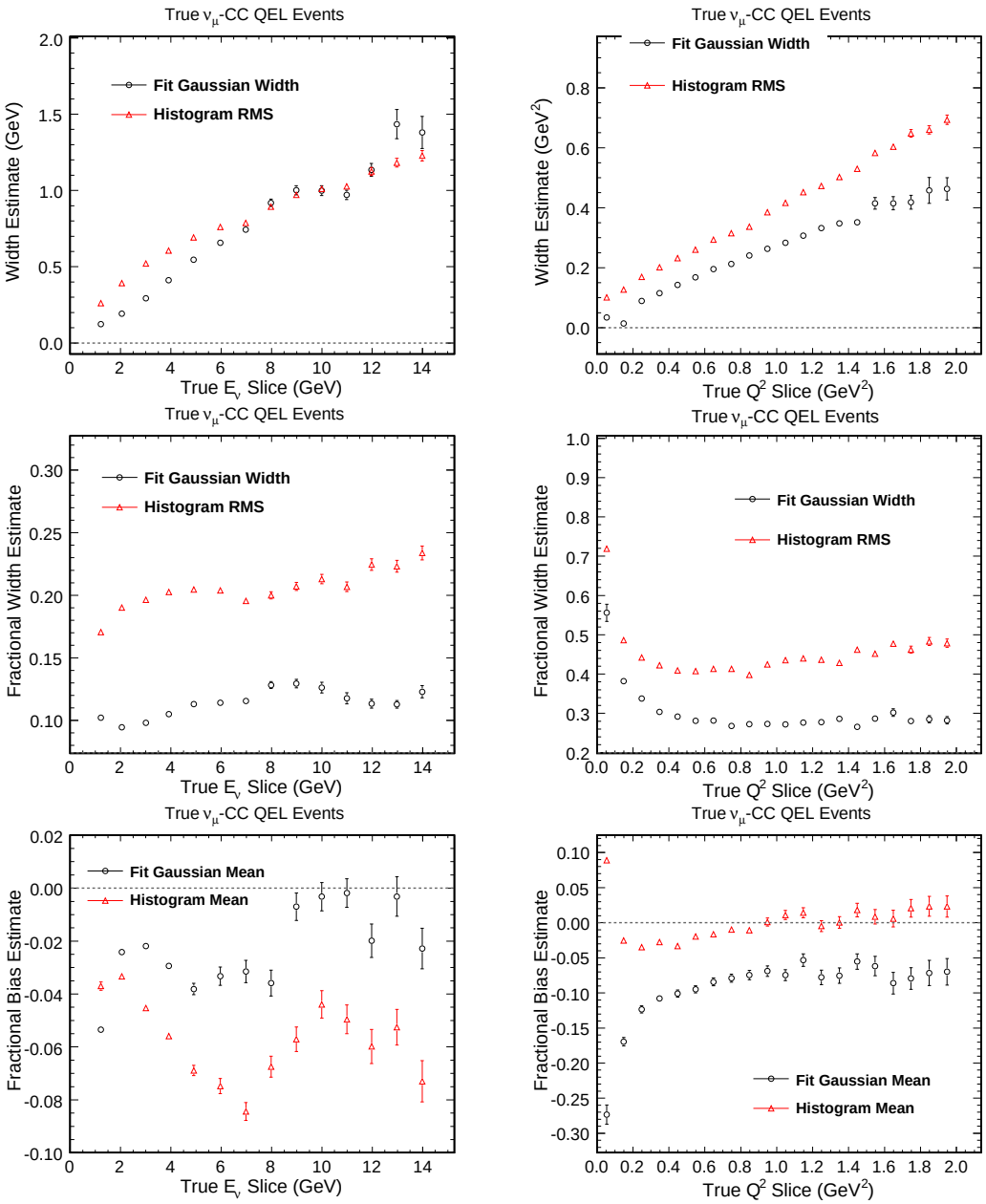

Figure 13: **QEL-assumed kinematic resolutions.** *All figures correspond to true ν_μ-CC QEL events with the left-hand figures showing the QEL-assumed neutrino energy and the right-hand figures showing the QEL-assumed squared four-momentum transfer. The top figures show the Gaussian widths from the log-normal fits to the $R-T$ distributions as black circles along with the RMS values of the $R-T$ histograms as red triangles. All points are plotted at the mean value of the true muon energy in a given slice rather than at the centre of that slice. The second row of figures show the fractional fitted Gaussian widths and $(R-T)/T$ histogram RMS values whilst the bottom row of figures show the fractional fitted Gaussian means and $(R-T)/T$ histogram means. The differences between the black circles and red triangles correspond to the influence of the tails of the $R-T$ or $(R-T)/T$ distributions.*